Instantaneous Mapping of Coherently Coupled Electronic Transitions and Energy Transfers in a Photosynthetic Complex Using Angle-Resolved Coherent Optical Wave-Mixing

Ian P. Mercer,[1] Yasin C. El-Taha,[2] Nathaniel Kajumba,[2] Jonathan P. Marangos,[2] John W. G. Tisch,[2] Mads Gabrielsen,[3] Richard J. Cogdell,[3] Emma Springate,[4] and Edmund Turcu[4]

[1]*School of Physics, Centre for Synthesis and Chemical Biology, University College Dublin, Dublin 4, Ireland*
[2]*Quantum Optics and Laser Science Group, Blackett Laboratory, Imperial College, London, United Kingdom*
[3]*Biochemistry and Molecular Biology, Faculty of Biomedical and Life Sciences, University of Glasgow, Glasgow, United Kingdom*
[4]*Central Laser Facility, STFC Rutherford Appleton Laboratory, Didcot, United Kingdom*

(Received 19 September 2008; published 6 February 2009)

Understanding the role of coherent electronic motion is expected to resolve general questions of importance in macromolecular energy transfer. We demonstrate a novel nonlinear optical method, angle-resolved coherent wave mixing, that separates out coherently coupled electronic transitions and energy transfers in an instantaneous two-dimensional mapping. Angular resolution of the signal is achieved by using millimeter laser beam waists at the sample and by signal relay to the far field; for this we use a high energy, ultrabroadband hollow fiber laser source. We reveal quantum electronic beating with a time-ordered selection of transition energies in a photosynthetic complex.

DOI: 10.1103/PhysRevLett.102.057402 PACS numbers: 78.47.Fg, 42.50.Md, 71.35.−y, 78.47.jm

Coherent optical four-wave mixing [1] with three laser pulses of variable delay has been used widely to obtain information on the time scales of energy transfer in complex molecular systems. However, the interpretation of these measurements is difficult, in particular, where chromophores are strongly coupled, such as in photosynthetic systems, and new methods are required that can distinguish between energy transfers and coherent electronic couplings. Significant progress has been made recently with the extension of photon echo four-wave mixing to deliver two-dimensional maps via heterodyned detection. This has been applied to systems ranging from small molecules [2] to semiconductors [3,4] and biological molecules, [5,6] and has recently provided strong evidence of a quantum beating between coherently coupled electronic transitions within a photosynthetic system at a temperature of 77 K [7]. With this approach, a coherent coupling of electronic transitions is predicted to give a synchronized modulation of feature amplitudes and widths for maps recorded as a function of an optical delay time [8]. This and other two-dimensional methods that are sensitive to electronic coherence, require signal accumulation times ranging from minutes to hours. Long exposure times can lead to photodegradation and toxicity for sensitive samples.

Here we demonstrate a powerful new nonlinear optical method, angle-resolved coherent (ARC) wave mixing, which separates out coherently coupled quantum transitions and energy transfers in a single projection image (map), without postprocessing. We show for the first time that the position of a feature can map uniquely to each of the four laser beam interaction energies that produce the signal. The power of the new method is demonstrated with the B800 and B850 pigments of the light harvesting complex II (LH2) of purple bacteria [9] at ambient temperature. For the first time, we directly observe a time ordering in the selection of transition energies for a quantum beating between coherently coupled electronic transitions.

Waist sizes of less than 100 μm are common in four-wave mixing in order to generate the light intensities required for efficient signal generation. In two-dimensional heterodyned four-wave mixing with a broad bandwidth laser, small waist sizes (giving high divergence) are also required in order to mask a variation in the angle of signal emission that will occur within the spatial profile of the heterodyning laser beam. This variation in angle will otherwise contribute to structure in the two-dimensional maps, reducing the amount of information that can be retrieved in conventional experiments [10]. In contrast, ARC wave mixing makes use of the angular distribution of the signal intensity and uses millimeter laser beam waists at the sample.

The direction of the signal emission in ARC four-wave mixing is given by conservation of momentum as $\underline{k}_S = -\underline{k}_1 + \underline{k}_2 + \underline{k}_3$ for laser photon momenta $\underline{k}_1, \underline{k}_2, \underline{k}_3$ and the generated signal $\underline{k}_S$ as is common in four-wave mixing. Figure 1(a) shows a configuration in which the emission is detected at the remaining vertex of the box formed by the three driving laser beams, with angles $\alpha_h = 2.1°$ and $\alpha_v = 1.8°$ between laser beams in the horizontal and vertical planes, respectively. Since the magnitude of each light vector is frequency dependent, the direction of scattered light depends on the frequencies (energies) selected from each laser beam, which are governed by the behavior of chromophores in the sample.

This variation in the emission direction is small. In our experiment, a signal feature is deviated by only 0.01° for a difference in wavelength between light interactions of 5 nm. To detect these small variations in angle, we use a 1 mJ, 30 fs titanium sapphire laser (repetition rate 1 kHz) with argon gas filled hollow fiber pulse compression

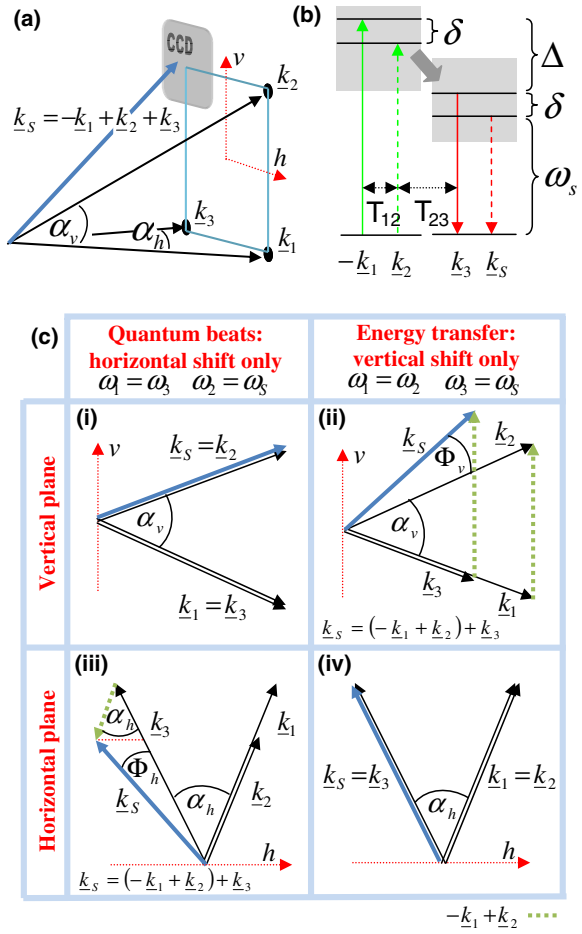

FIG. 1 (color online). Illustration of ARC four-wave mixing, showing: (a) the laser beam layout without use of a diffractive optic; (b) the time-ordered light-matter interaction sequence evidenced for B850 in this experiment, for which solid and dashed lines represent real and conjugate light-field interactions that combine in pairs to represent a photon exchange, and where T_{12} and T_{23} represent times between light-field interactions; (c) representation of orthogonal signal deviations for an electronic quantum beat and an energy transfer.

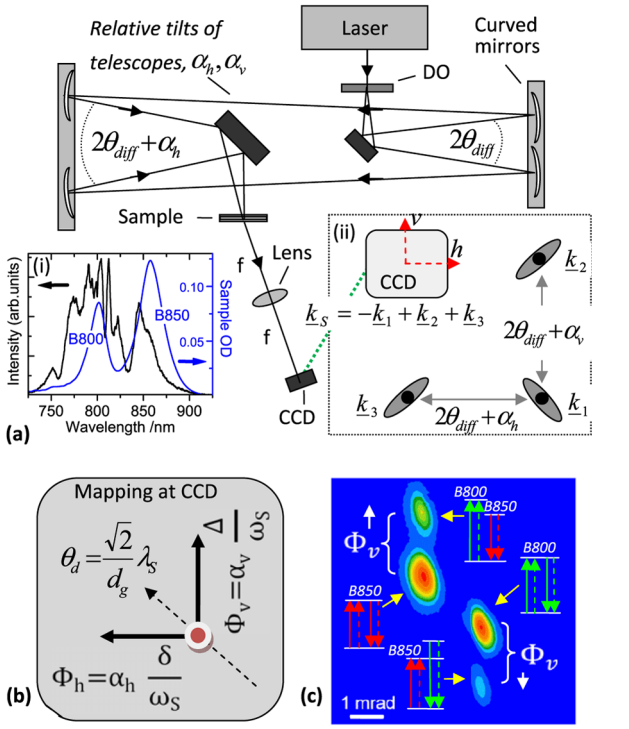

FIG. 2 (color online). Illustration of the experiment apparatus, showing: (a) the optical layout with a diffractive optic (DO) and telescopes, for which the focal lengths of the lens (f) and curved mirrors are 500 mm and 400 mm, respectively, in experiment. Shown inset are the measured spectra of laser intensity and sample absorption (optical density, OD), and the laser beam distribution at the detector which forms a box geometry; (b) an illustration of the ARC-TG signal mapping at the detector; (c) a measured ARC-TG map of LH2 at a time delay of 1.3 ps. Two CCD images are summed from optical filtering at (800+/−5) nm and (852+/−5) nm, with intensity in arbitrary units.

[11,12]. The coherent bandwidth from the hollow fiber spans the range 750 to 880 nm, as required to excite both B800 and B850 pigments [Fig. 2(a), inset i]. The pulse duration at the sample is measured to be (35+/−5) fs. This is less than an effective pulse duration of 230 fs that results from the tilt of the pulses ($\alpha_{h,v}$) and as such, effort is not made to compress the pulses further. The hollow fiber provides inherent spatial stability combined with a near to diffraction limited output, which is attenuated to give 1.1 μJ/pulse at the sample. This energy is up to 3 orders of magnitude greater than that in conventional experiments, permitting the use of a large laser beam waist on the order of millimeters at the sample while maintaining the light intensity required for efficient signal generation. This minimizes the beam spreading effects of diffraction and permits detection of the emitted signal with high angular resolution using a two-dimensional CCD detector placed in the optical far field of the sample.

The ARC methodology may be applied to four and higher order wave mixing schemes, to both the transient grating (TG) and echo pulse sequences and, to resonant and nonresonant interactions spanning the optical spectrum. Here the resonant TG four-wave mixing sequence is applied, in which pulses 1 and 2 are precisely overlapped in time and pulse 3 arrives with a controllable delay. Figure 1(b) shows a light-matter interaction for this sequence that involves an energy transfer with a quantum defect, $\Delta = \omega_1 - \omega_3 = \omega_2 - \omega_S$ and a coupled coherence between two electronic transitions with a difference in energy, $\delta = \omega_1 - \omega_2 = \omega_3 - \omega_S$.

Figure 1(c) illustrates that a vertical deviation in signal emission results from a difference in the interaction frequencies of beams 1 and 3 (finite Δ) corresponding to an energy transfer. This is uncoupled from a horizontal deviation in signal emission that results from a difference in the interaction frequencies of beam 1 and 2 (finite δ), corresponding to a coherent excitation of two coupled single

electron transitions (a quantum electronic beating). The ability to deliver both the magnitudes and signs of Δ and δ derives from spatially extended interferences in the sample given by $-\underline{k}_1 + \underline{k}_2$ and ensembles of identically emitting molecules are distinguished according to these interferences.

We calculate the signal deviation as a function of the selected laser beam frequencies by three-dimensional numerical ray-vector addition. The angle of signal deviation is also readily derived from Fig. 1(c) in the small angle approximation. For energy transfer, $|\underline{k}_1| = |\underline{k}_2|$ and the magnitude of $-\underline{k}_1 + \underline{k}_2$ in the vertical plane as illustrated in Fig. 1(c) (ii) is given by both $\omega_2\alpha_v$ and $\omega_S(\alpha_v + \Phi_v)$ which when equated simplifies to $\Phi_v = \alpha_v\Delta/\omega_S$, consistent with previous work [13]. This can be visualized as the scattering of beam 3 from a stationary population grating (of $\sim$10 μm period). For quantum electronic beats, $|\underline{k}_1| \neq |\underline{k}_2|$ and a projection of $-\underline{k}_1 + \underline{k}_2$ in the horizontal plane as illustrated by the red line in Fig. 1(c) (iii), is given by both $\omega_S\Phi_h$ and $(\omega_1 - \omega_2)\alpha_h$ which when equated simplifies to $\Phi_h = \alpha_h\delta/\omega_S$. This can be visualized as the scattering of beam 3 from propagating modulations in the sample polarization (of a millimeter period).

To resolve signal emission in ω_s, enabling a full ARC map to be obtained with a single laser pulse, we impart an angular dispersion on the emission along the diagonal. This is performed by the robust and straightforward apparatus shown in Fig. 2(a). A single diffractive optic, effectively comprising two orthogonal diffraction gratings of 30 μm period, produces four first-order diffracted laser beams from a single laser source and directs these beams into a box geometry. One beam is blocked and the remaining three are relayed to the sample by three telescopes which are arranged with the diffractive optic and the sample at common object and image points. The use of parallel aligned telescopes ($\alpha_h = \alpha_v = 0$) gives sensitivity to ω_s only. Full ARC mapping is given by imparting a relative tilt (finite α_h and α_v) between the laser beams within the telescopes while keeping the same object and image points.

Figure 2(a) (inset ii) illustrates the angular dispersion of each laser beam along the respective diagonals of the box geometry. Angle deviations in both the horizontal and vertical planes are given by the diffraction equation, $\theta_{\text{diff}} = \lambda_S/d_g$ for a wavelength, λ_S and a grating ruling separation, d_g. As a result, the dimensions of the box geometry increases with wavelength, providing a mapping of the signal emission along a diagonal, $\theta_d = \sqrt{2}\lambda_S/d_g = 2\sqrt{2}\pi c/\omega_S d_g$. Figure 2(b) illustrates how the position of the detected signal maps to λ_S, Δ, and δ. Serving as a demonstration measurement, Fig. 2(c) shows the overlay of two consecutive ARC-TG maps of LH2 taken with optical band-pass filtering (10 nm bandwidths) of the signal at 800 nm and 852 nm. A delay time of 1.3 ps allows for the relaxation of electronic coherences ($\delta \sim 0$). The 852 nm filtered emission is shifted diagonally from that of the 800 nm filtered emission, as expected from Fig. 2(b). The measured vertical displacements of +2.05 and −1.90 mrad between features correspond to $\Delta = \pm 770$ cm^{-1} for downhill (Φ_v and Δ positive) and uphill (Φ_v and Δ negative) transfer, respectively. This is consistent with energy transfer being derived from the peak excitations determined for B800 and B850.

The sample (detergent isolated complexes of LH2 *Rps. acidophila* strain 10050) is of thickness 100 μm, which in combination with the small beam angles in this experiment ensures that phase matching effects [1,14] do not contribute significantly to our experiment. All figures shown are for an excitation probability of 0.1 per pigment, given by a laser pulse energy of 1.1 μJ/beam at the sample within a beam waist of 4.1 mm.

Figure 3(a) shows an ARC-transient grating signal measured as a function of time delay without optical band-pass filtering at the detector. From this figure, a single ultrafast laser pulse is deduced to be sufficient to deliver a full two-

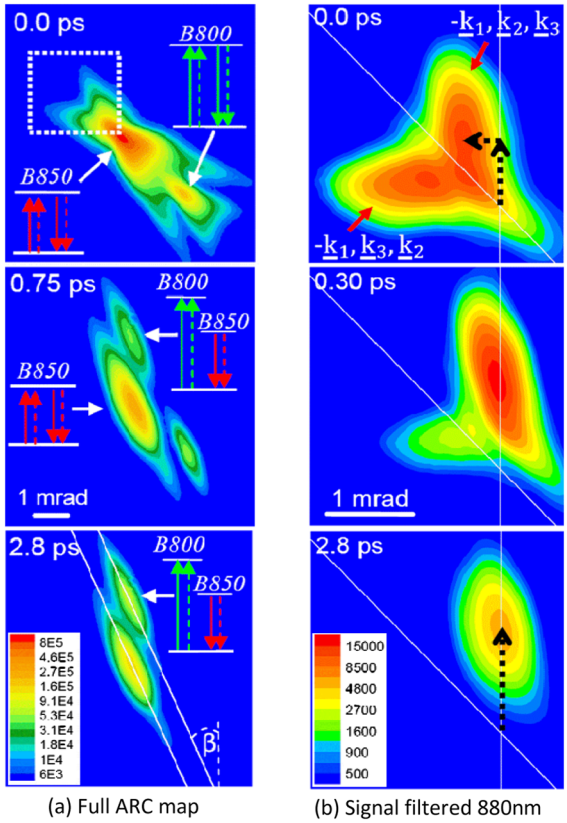

FIG. 3 (color online). Measured ARC-TG maps of LH2 for pulse time delays as labeled, showing: (a) full maps overlaid with lines at $\beta = 25.0°$, positioned to overlay features at longest delay; (b) maps with signal band-pass filtering at 880 nm (10 nm bandwidth), overlaid with a vertical and a 45° diagonal line, and with illustration of the feature displacements (dotted arrows) associated with Δ and δ. A box shown in (a) illustrates the position of the frame for figure (b). Color representations are in detector counts per pixel for an Andor DV420 CCD integrated over 200 ms (200 laser pulses) with our apparatus, and accounts for neutral density attenuation filters at the detector used to avoid detector saturation.

dimensional ARC image. Features resulting from B800 and B850 intrapigment transfers are displaced along the diagonal as expected from Fig. 2. A symmetry of the map about the diagonal at zero time delay results from the symmetry of the laser beam arrangement about the diagonal where the pulses of laser beams 2 and 3 are precisely overlapped in time. This symmetry is lifted with the delay of beam 3 relative to beams 1 and 2, giving the TG interaction time ordering. The emission from B800 is reduced with time delay and a new, off-diagonal feature emerges due to energy transfer from B800 to B850. A measured 0.8 ps lifetime for the energy transfer out of B800 agrees with standard TG measurement [15]. Features are observed to be aligned to an angle of $\beta = 25.0°$ from the vertical at long time delay (as overlaid). This angle of orientation is calculated assuming that a range of emission energies are derived from a single excitation energy (homogenized energy reorganization, $d\omega_a/d\omega_S = 0$).

Figure 3(b) shows the measured ARC-TG with 10 nm bandwidth filtered detection at $\lambda_S = 880$ nm ($11\,360$ cm^{-1}), overlapping the maximum of B850 fluorescence. This feature is attributed to energy transfers within the B850 pigment. As in Fig. 3(a), reflection symmetry is seen about the diagonal at zero time delay, with the upper feature resulting from the TG interaction time ordering (as labeled). This feature is displaced vertically upwards by 0.73 mrad and horizontally to the left by 0.38 mrad, corresponding to $\Delta = +260$ cm^{-1} and $\delta = +120$ cm^{-1} [see Fig. 2(b)]. This feature persists with the delay of beam 3 and translates progressively to the right. At a time delay of 2.8 ps, its vertical displacement from the diagonal is 1.1 mrad ($\Delta = +400$ cm^{-1}) corresponding to a peak excitation at 849 nm.

The displacement of this feature corresponds to a value of δ that decreases with a single exponential time constant of 160 fs. This time constant is equivalent to the decay time measured for the three-pulse photon echo peak shift (3PEPS) in B850 [16]. It is not possible with a 3PEPS measurement to directly distinguish the contributions from coherent electronic coupling (excitons) from that of intrapigment energy transfers. With the ARC-TG, we observe this time scale of energy reorganization in B850 to be characterized by an ordered reduction in a beat frequency between coherently coupled electronic transitions (exciton transitions).

All of the laser beam and scattered light interaction energies can be derived from an ARC measurement of δ, Δ and ω_S [see Fig. 1(b)]. For example, deduced for the feature in Fig. 3(b) at zero delay time is $\omega_1 = 11\,740$ cm^{-1}, $\omega_2 = 11\,620$ cm^{-1}, $\omega_3 = 11\,480$ cm^{-1} and $\omega_S = 11\,360$ cm^{-1}. Given that the third interaction necessarily precedes the final scattering, the observed direction for this feature displacement requires a downward time ordering of the third and scattered light-matter interaction energies. No equivalent feature shift is observed to the right at zero delay time, as would result from an upward time ordering. At a time delay of 2.8 ps, $\omega_1 = \omega_2 = 11\,760$ cm^{-1} and $\omega_3 = \omega_S = 11\,360$ cm^{-1} representing a population state.

In conclusion, ARC wave mixing provides a powerful new methodology to inform quantum molecular simulation [17–19] on the mechanisms by which excitations explore the most efficient path for energy transfer and relaxation. For the first time, we distinguish quantum beatings from energy transfers as horizontal and vertical shifts in a direct projection. In doing so, we directly reveal a time-ordered selection of transition energies for the excitation of a coherent superposition of electronic states (quantum beating) in a macromolecule. We observe the subsequent relaxation to be characterized by a reduction in the superposition beat frequency. We show the ability to project maps in a single laser pulse such that full information can be gathered prior to chemical change in the sample resulting from an exposure to light, for example, via denaturization or isomerization. With the combined advantages of speed and sensitivity to electronic function, opportunities with ARC wave mixing lie in rapid sample characterization and the investigation of unstable samples.

We acknowledge the support of EPSRC and BBSRC and the EU Framework 6 Lab Share programme.

[1] S. Mukamel, *Principles of Nonlinear Optical Spectroscopy* (Oxford University Press, New York, 1995).
[2] J. D. Hybl, A. A. Ferro, and D. M. Jonas, J. Chem. Phys. **115**, 6606 (2001).
[3] X. Li *et al.*, Phys. Rev. Lett. **96**, 057406 (2006).
[4] T. Zhang *et al.*, Proc. Natl. Acad. Sci. U.S.A. **104**, 14 227 (2007).
[5] S. Kim *et al.*, J. Phys. Chem. B **112**, 10 054 (2008).
[6] C. Fang *et al.*, Proc. Natl. Acad. Sci. U.S.A. **105**, 1472 (2008).
[7] G. S. Engel *et al.*, Nature (London) **446**, 782 (2007).
[8] A. V. Pisliakov, T. Mancal, and G. R. Fleming, J. Chem. Phys. **124**, 234505 (2006).
[9] R. J. Cogdell, A. Gall, and J. Kohler, Q. Rev. Biophys. **39**, 227 (2006).
[10] M. K. Yetzbacher *et al.*, J. Chem. Phys. **126**, 044511 (2007).
[11] M. Nisoli, S. D. Silvestri, and O. Svelto, Appl. Phys. Lett. **68**, 2793 (1996).
[12] J. S. Robinson *et al.*, Appl. Phys. B **85**, 525 (2006).
[13] T. J. Butenhoff and E. A. Rohlfing, J. Chem. Phys. **98**, 5460 (1993).
[14] N. Belabas and D. M. Jonas, J. Opt. Soc. Am. B **22**, 655 (2005).
[15] J. M. Salverda *et al.*, J. Phys. Chem. B **104**, 11 395 (2000).
[16] R. Agarwal *et al.*, J. Phys. Chem. A **106**, 7573 (2002).
[17] I. P. Mercer, I. R. Gould, and D. R. Klug, J. Phys. Chem. B **103**, 7720 (1999).
[18] G. D. Scholes *et al.*, J. Phys. Chem. B **103**, 2543 (1999).
[19] R. C. Walker *et al.*, J. Comput. Chem. **28**, 478 (2007).